5-2020

Structural and Functional Characterization of Mitochondria with tRNA Mutations

Brooke Henry

Structural and Functional Characterization of Mitochondria with tRNA Mutations

An Honors Thesis submitted in partial fulfilment of the requirement of Honors Studies in Biology

By

Brooke Henry

Spring 2020

Biology

J. William Fulbright College of Arts and Sciences.

The University of Arkansas

Acknowledgements

I wish to thank everyone who has aided in my research project, though they all may not be named. I wish to acknowledge their contributions, as they are highly appreciated. I am deeply grateful for the following:

Dr. Shilpa Iyer for allowing me to work in her lab and providing me the opportunity to pursue a research project under her mentorship. Ajibola B. Bakare and Joshua Stabach for their constant support and direction in my research.

I am grateful for the University of Arkansas Honors College, the University of Arkansas Department of Biology for the opportunity and support to conduct undergraduate research.

I am grateful to the United States Department of Defense for providing funding of my project.

I am grateful to Dr. Shilpa Iyer, Dr. Michael Lehmann, Dr. Frank Millet, and Dr. Susan M. Marren for their willingness to serve on my thesis committee.

Finally, I would like to thank my family and friends for supporting me throughout this project and my academic career.

Table of Contents

Abstract

Mitochondrial encephalopathy, lactic acidosis, and stroke-like episodes (MELAS) is one of the most common disorders associated with mitochondrial tRNA mutations. One of the most common causes of MELAS is mutation in the MT-TL1 gene which codes for mitochondrial tRNA Leucine (UUR). Mutation in MT-TE gene, another mitochondrial gene which encodes for mitochondrial tRNA Glutamate (GAA/G), has been implicated in various mitochondrial related myopathies. It remains unclear how point mutations in these tRNA genes result in disease onset and progression. Here, we report an early comparative analysis of fibroblast cell lines derived from patients carrying two different tRNA mutations: m.3243A>G and m.14739G>A. This study examines the relationship between mitochondrial structure and function as it relates to disease onset and severity. Morphological analysis revealed differences in network structure between the tRNA mutant and control cell lines. This was correlated with a decrease in mitochondrial function as indicated by aberrant mitochondrial membrane potential and Reactive Oxygen species production. Results from this study suggest that mitochondrial tRNA mutations can result in dysregulation of mitochondrial morphology, consequently affecting mitochondrial function.

Abbreviations

mtDNA	Mitochondrial Deoxyribonucleic acid
tRNA	Transfer RNA
ATP	Adenine Tri-Phosphate
tRNA	Transfer RNA
FCCP	Carbonyl cyanide p- (tri-fluromethoxy) phenyl-hydrazone
MEM	Minimal Essential Media
mt-tRNA-Leu	Mitochondrial tRNA specific for Leucine
mt-tRNA-Glu	Mitochondrial tRNA specific for Glutamic Acid
MMP	Mitochondrial Membrane Potential
ROS	Reactive Oxygen Species
dPBS	Dulbecco's Phosphate Buffered Saline
TMRE	Tetramethylrhodamine, ethyl ester
ROI	Region of interest

Introduction

Mitochondria are important to many cellular functions including ATP synthesis, apoptosis, calcium buffering, and reactive oxygen species production. Mitochondria contain their own DNA (mtDNA), but the majority of mitochondrial proteins are synthesized by nuclear DNA (El-Hattab, Adesina, Jones, & Scaglia, 2015). Mutations in either the mitochondrial DNA (mtDNA) or nuclear DNA regions related to mitochondrial function can cause disease. The phenotype of mitochondrial disease varies widely depending on the nature of the genetic mutation. The type of mutations that this paper will focus on are those that affect transfer RNAs (tRNAs) in the mitochondria. tRNA mutations make up 10% of the mtDNA genome but are present in 60% of adults with a mtDNA disease (Queen, Steyn, Lord, & Elson, 2017).

The mitochondrial genome encodes 22 tRNAs, one for each amino acid and a second for both the tRNA for Leucine and the tRNA for Serine (Scaglia & Wong, 2008). tRNA encoded by the mitochondrial genome exhibits similar functions to nuclear-encoded tRNA (Queen et al., 2017); they bring amino acids to the ribosomal complex in order to synthesize proteins (Scaglia & Wong, 2008). tRNA molecules maintain a secondary structure of a clover leaf which then folds to form an L-shape. This 3D L-shape is held together by tertiary interactions (Queen et al., 2017). This structure allows the tRNA to carry out its functions within the cell.

In this study, we sought to understand the effect of tRNA mutations on mitochondrial structure and function using two human fibroblast cell lines with mitochondrial tRNA mutations as our model. The first (SBG6) is the m.3243A>G

mutation in which a guanine base has been substituted by an adenine base at the mitochondrial genome location 3243. This nucleotide equates to nucleotide 14 within the mitochondrial tRNA molecule for the amino acid Leucine (mt-tRNA-Leu(UUR)) (Queen et al., 2017). This error leads to Mitochondrial encephalopathy, lactic acidosis, and stroke-like episodes, or MELAS syndrome, one of the most frequent maternally inherited diseases (El-Hattab et al., 2015). This disease has two categories: one with frequent seizures, headaches, and vomiting, while the other may include high lactic acid buildup and myopathy. This mutation is present in 80% of MELAS patients (El-Hattab et al., 2015). Interactions between bases in tRNA is very important for maintaining the tertiary structure. The m.3243A>G mutation alters the tertiary structure of mt-tRNA-Leu(UUR), which impairs mitochondrial translation (Queen et al., 2017) and decreases overall mitochondrial respiration. The second cell line (SBG7) is m.14739G>A. At location 14739 in the mitochondrial genome, the guanine has been replaced by an adenine. This mutation affects the function of the tRNA specific for glutamic acid (mt-tRNA-Glu) by unknown mechanisms to cause mitochondrial pathology. These tRNA mutations can in turn affect many respiratory chain enzymes, leading to diseased phenotypes (Koga, Hodges, Markin, & Gorman, 1995).

Fibroblast Sample	Gene affected	tRNA Affected	Mutation
Control (BJSI)	Normal	N/A	N/A
SBG6	MT-TL1	mt-tRNA-Leu (UUR)	m.3243A>G
SBG7	MT-TE	mt-tRNA-Glu (GAA/G)	m.14739G>A

Table 1. Cell lines and their corresponding mutations. Table showing diseased and control cell lines with their corresponding mutation and which tRNA is affected

Mitochondria go through rounds of fission and fusion to maintain metabolic demands of cells. (Ni, Williams, & Ding, 2015). Mitochondrial fission is the division of one mitochondrion into two daughter mitochondria, whereas fusion combines two mitochondria into one mitochondrion. These processes must be in balance in order to have a well-functioning mitochondrial network. It has been suggested that the diseased mitochondria may have activated fission or deactivated fusion so that the damaged mitochondria will not be able to incorporate back into the mitochondrial network (Ni et al., 2015). A hyper-fused mitochondrial network or a fragmented mitochondrial network indicates an imbalance in fission and fusion cycles, which can an indication of mitochondrial disease. In this study, a novel technique, Mitochondrial Network Analysis (MiNA) was used to characterize mitochondrial morphology in diseased and control fibroblast cell lines.

We hypothesize that these diseased cell lines will display an altered morphology, with a subsequent alteration in mitochondrial function. Functional analysis of mitochondria was assessed by recording Mitochondrial Membrane Potential (MMP) and Mitochondrial Reactive Oxygen Species (mitoROS) production in diseased and healthy control fibroblast cell lines. Mitochondria maintain a membrane potential across the inner mitochondrial membrane in order to drive ATP synthesis (Cadenas, 2018). The complexes of the respiratory chain create this gradient by pumping protons across the inner mitochondrial membrane (Chen, 1988). This study uses mitochondrial inhibitors FCCP (Carbonyl cyanide 4-(trifluoromethoxy)phenylhydrazone; Sigma, U.S.A) and Oligomycin to create an environment of mitochondrial stress. FCCP is a potent mitochondrial uncoupler. It uncouples oxidation and phosphorylation by destabilizing the

proton gradient (Brennan et al., 2006). Oligomycin inhibits ATP synthase by blocking its proton channel, subsequently hyperpolarizing the mitochondria (Fernyhough & McGavock, 2014).

Mitochondria are considered the main source of cellular ROS, with superoxide ($O_2^{\bullet -}$) as the primary type (Murphy, 2009). ROS are important for redox signaling, but can also cellular damage. Superoxide is produced by a one-electron reduction of oxygen (O_2) and is predominantly produced by Complex I and Complex III of the respiratory chain (Murphy, 2009). Complex I reduces NADH into NAD+ and passes two electrons to ubiquinone. It also pumps four protons across the inner mitochondrial membrane. Complex III passes electrons to cytochrome C and also pumps four protons across the inner membrane (Nicholls & Ferguson, 2013). This study uses mitochondrial inhibitors Rotenone and Antimycin A to induce mitochondrial stress. Rotenone inhibits Complex I near the binding site for ubiquinone, so electrons cannot be further passed down the electron transport chain. It has been shown to increase ROS production from Complex I (Gupta & Milatovic, 2014). Antimycin A inhibits the Q_i center of Complex III and has been shown to release ROS inside and outside of the mitochondria (Quinlan, Treberg, & Brand, 2011).

Our results suggest that the morphology of the mitochondrial network is altered in tRNA mutants, but it is unclear if it exhibits a hyper-fused or hyper-fragmented morphology. Functional analysis suggests that tRNA mutant cell lines display decreased function in regard to mitochondrial membrane potential, but ROS production is unclear.

Methods and Materials

Cell Culture:

Control and diseased fibroblast cell (see Table 1) lines were thawed and maintained in culture until passage 8. All cells were maintained in Minimal Essential Media (Gibco, U.S.A) supplemented with 10% Fetal Bovine Albumin (Hyclone, U.S.A) and 2mM L-Glutamine (Thermo Fisher Scientific , U.S.A). Cells were cultured and maintained at $37^{o}C$ in a humidified atmosphere of 5% CO_2 following established protocols.

Cell Imaging:

A day prior to experiment, cells were seeded in 35 mm^2 dishes and incubated overnight. On the day of the experiment, culture media was aspirated and cells were washed with dPBS (Dulbecco's Phosphate Buffered Saline). The FCCP (Sigma, U.S.A) treatment group was treated with 0.7 µM FCCP solution and incubated (in a $37^{o}C$, 5% CO_2 incubator) for 30 minutes. The media was then aspirated off and 150nM MitoTracker Red CM-H2Xros (Thermo Fisher Scientific, U.S.A) was added, followed by 30 minutes of incubation. Cells were washed again with dPBS and Nucblue (Thermo Fisher Scientific, U.S.A) solution (nuclear stain) was added, followed by an additional 20 minutes of incubation. At the end of the incubation period, cells were washed with 2-3 times with dPBS to remove excess stain. Fluorescent and phase contrast images were acquired at 40X magnification for each dish and cell line using EVOS FL microscope. The images were taken under red fluorescent protein (RFP; 60% and 250ms exposure and exposure time), DAPI (20% and 120ms), and phase contrast channels. Approximately 5-7 images

were taken per dish, with 5 dishes per cell line and treatment group. These images were saved for further analysis.

Mitochondrial Network Analysis (MiNA) using ImageJ

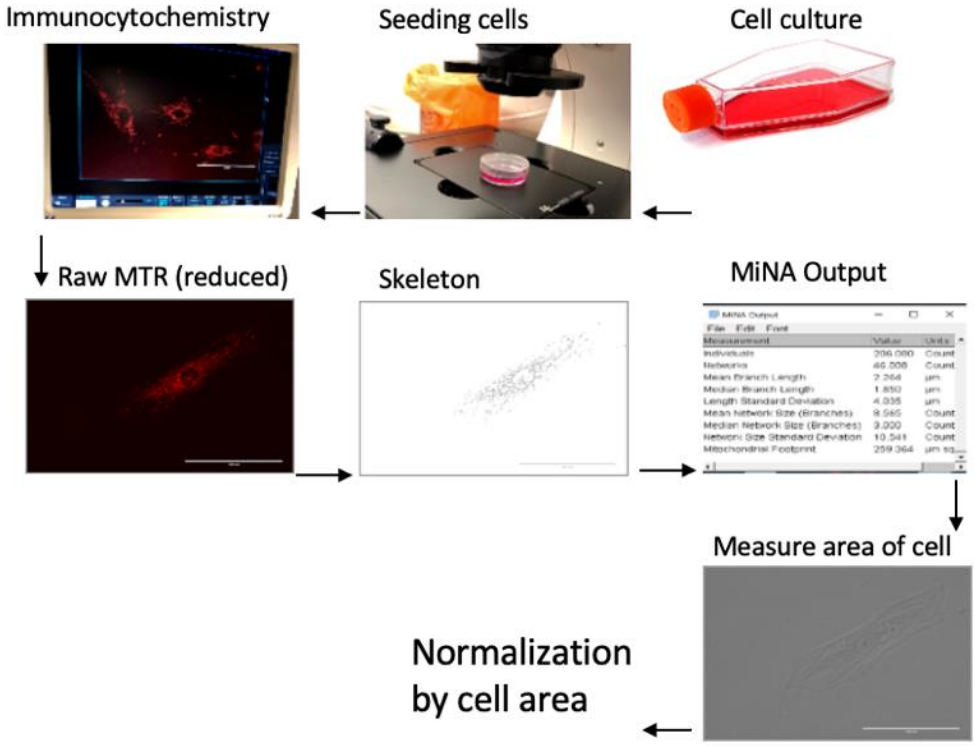

Figure 1. Visual diagram of MiNA procedure. Representation of staining and imaging fibroblast cells using MitoTracker Red CM-H2Xros, followed by analysis using the MiNA ImageJ protocol.

Cell images were analyzed using the NIH's open source image analysis software ImageJ. This allows the intensity of the stain in cell images to be converted to numerical data. Processing of the images involved subtracting the background, enhancing local contrast, making the image binary, and skeletonizing (see Figure 1). This converts the cell image into a 2-dimensional map of the mitochondrial network. Adobe Photoshop CC 2018 was used to isolate individual cells. The individual cell skeletons were then analyzed using the

Mitochondrial Network Analysis (MiNA) plugin for ImageJ. This software creates numerical data related to the morphology of the mitochondria. The parameters include mitochondrial individuals, networks, mean branch length, mean network size (see Table 2). Total respiring mitochondria was calculated by adding the number of individuals to number of networks. Each cell was outlined in ImageJ to determine its area. The MiNA parameter values for each cell were divided by the total cell area in order to normalize the data. Mean and standard deviation (S.D) were calculated from the data. Values outside of the 2S.D range were excluded from the data set as outliers.

MiNA Parameter	**Definition**
Individuals	Number of objects without nodes
Networks	Number of objects with at least one node
Mean Branch Length	Average length of branches
Mean Network Size	Average number of branches per network.

Table 2. MiNA parameters and definitions. Table showing each MiNA parameter along with its respective definition (Valente, Maddalena, Robb, Moradi, & Stuart, 2017).

Flow cytometry:

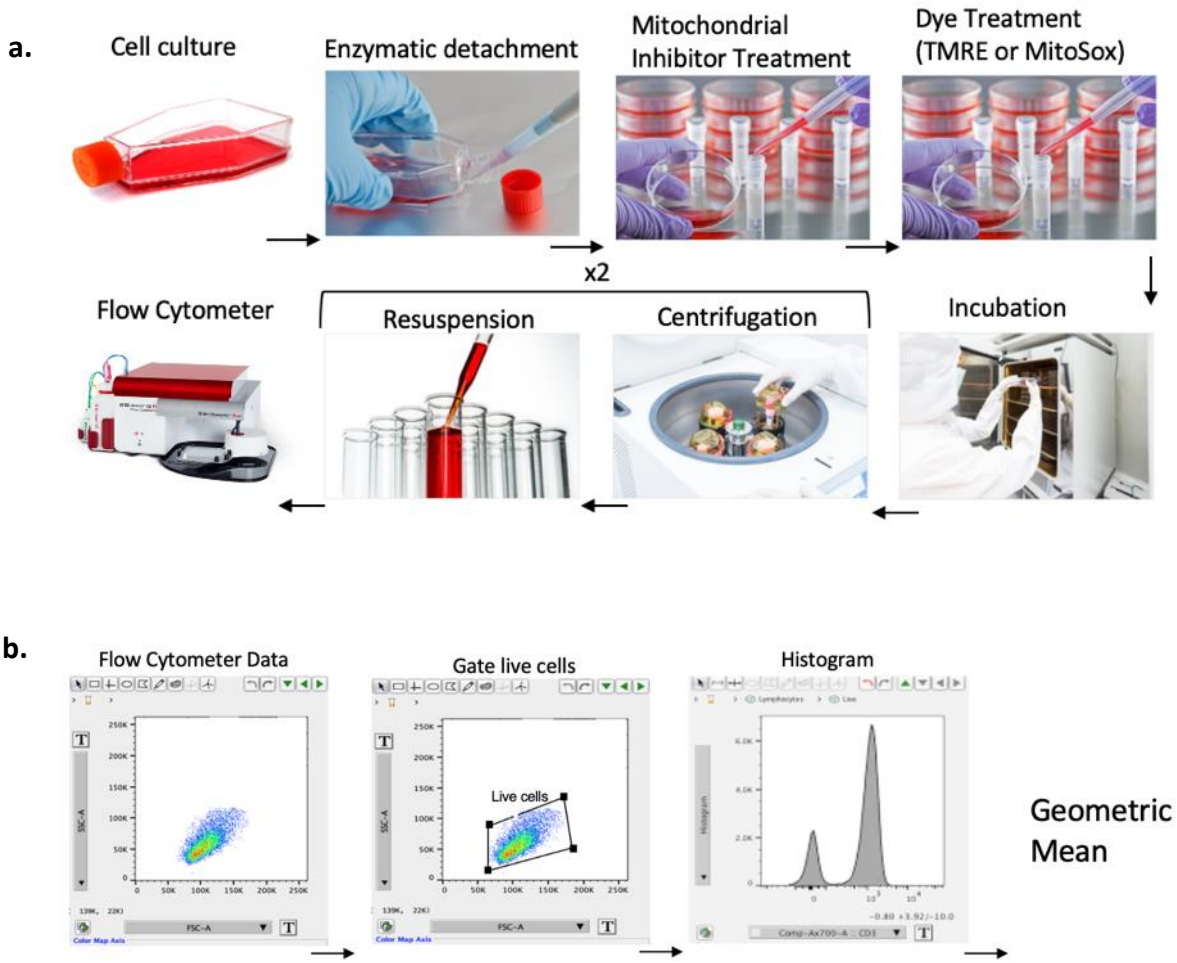

Figure 2. Visual diagram of flow cytometry procedure and data analysis. Representation of flow cytometry protocol (a) including cell culture, treatment, and preparation. Representation of data analysis using FlowJo (b) including gating the live cells, creating a histogram, and performing geometric mean to measure mean fluorescent intensity.

Cells were grown until approximately 80% confluence. On the day of the experiment, cells were enzymatically detached and divided into their respective treatment groups. The treatment groups for the membrane potential (MMP) experiments are as follows: Non-Treated, TMRE (Tetramethylrhodamine, ethyl ester; Abcam, U.S.A) only, TMRE+FCCP, and TMRE +Oligomycin (Sigma, U.S.A). The final well concentrations of 50nM TMRE, 20µM FCCP, and 5µ M Oligomycin were applied to the respective

cells. The treatment groups for mitochondrial Reactive Oxygen Species (mitoROS) experiments are as follows: Non-treated, MitoSox (Thermo Fisher Scientific, U.S.A)only, MitoSox+Rotenone, and MitoSox+AntimycinA). Final well concentrations of 3µM MitoSox, 5µM Rotenone, and 5µM AntimycinA were applied to the respective cells.

In both the MMP and MitoROS experiments, the cells were treated with the respective mitochondrial inhibitors (FCCP, Oligomycin, Rotenone, and AntimycinA) 10mins prior to treatment with either TMRE (MMP) or MitoSox (MitoROS). After which incubation for 25mins followed. At the end of the incubation period, cells were centrifuged and resuspended in dPBS to get rid of excess stain. The cells were centrifuged a second time and resuspended in phenol-Red free MEM and transferred to Accuri C6 Flow cytometer for data acquisition, 10, 000 events was recorded for each well. Flow cytometry data was analyzed using FlowJo_V10 software. The non-treated group was used to gate for live cells and positive cell populations. The geometric mean, a measure of mean fluorescence intensity was determined, this value was multiplied with the counts for TMRE/MitoSox positive populations to normalize the data.

Immunocytochemistry:

Prior to experiment, 25,000 cells were seeded in 35mm$_2$ dishes overnight. On the day of the experiment, cells were treated with mitochondrial inhibitors and stained with the appropriate dye (TMRE or MitoSox). The cells were imaged at 40x, 3-5 images were acquired/dish. ImageJ was used to quantify the fluorescence intensity of the images. The integrated density, a measure of fluorescence intensity, was then divided by the area of the image in a specific region of interest (ROI). Three ROI measurements were taken

from dark backgrounds, in which no cells were located to determine the background intensity. These ROI measurements were divided by their area as well. An average of the background fluorescence intensity was taken and subtracted from those of the cells to normalize the data.

Statistical Analysis:

All statistics and graphs were performed using GraphPad Prism 8. One-way ANOVA with post-hoc Tukey was performed with an alpha value of 0.05 to determine statistical significance.

Results

Mitochondrial Morphology is perturbed in tRNA mutant cell lines:

To test the hypothesis that tRNA mutation affects mitochondrial morphology, we used MiNA to analyze mitochondrial structure and found that the number of individuals (Fig. 4a) and the number of networks (Fig. 4c) in SBG6 and SBG7 was significantly lower than the control cell line in the presence and absence of FCCP. The mean branch length (Fig. 4b) in SBG7 was significantly higher than the control line in the presence of FCCP. The mean network size (Fig. 4d) of SBG7 was significantly lower than the control cell line in the presence and absence of FCCP.

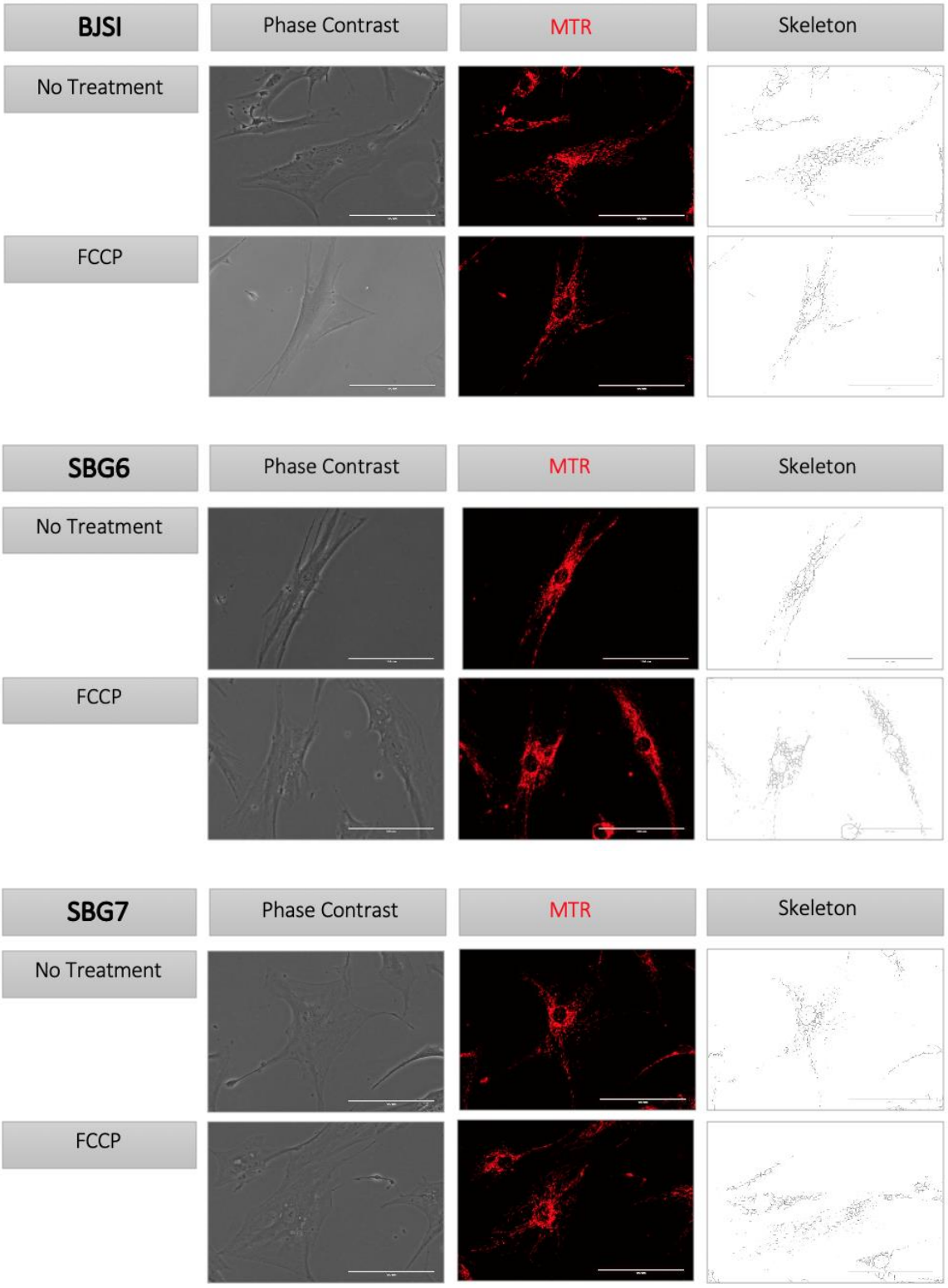

Figure 3. Fluorescent images of the mitochondrial network of diseased and control cell lines in the presence and absence of the mitochondrial uncoupler FCCP.

Fibroblast cells images from diseased and control cell lines stained with MitoTracker Red CM-H2Xros and taken under phase contrast and Red Fluorescent Protein (RFP) channels in the presence and absence of FCCP, followed by the skeletonized image of the fibroblast cell.

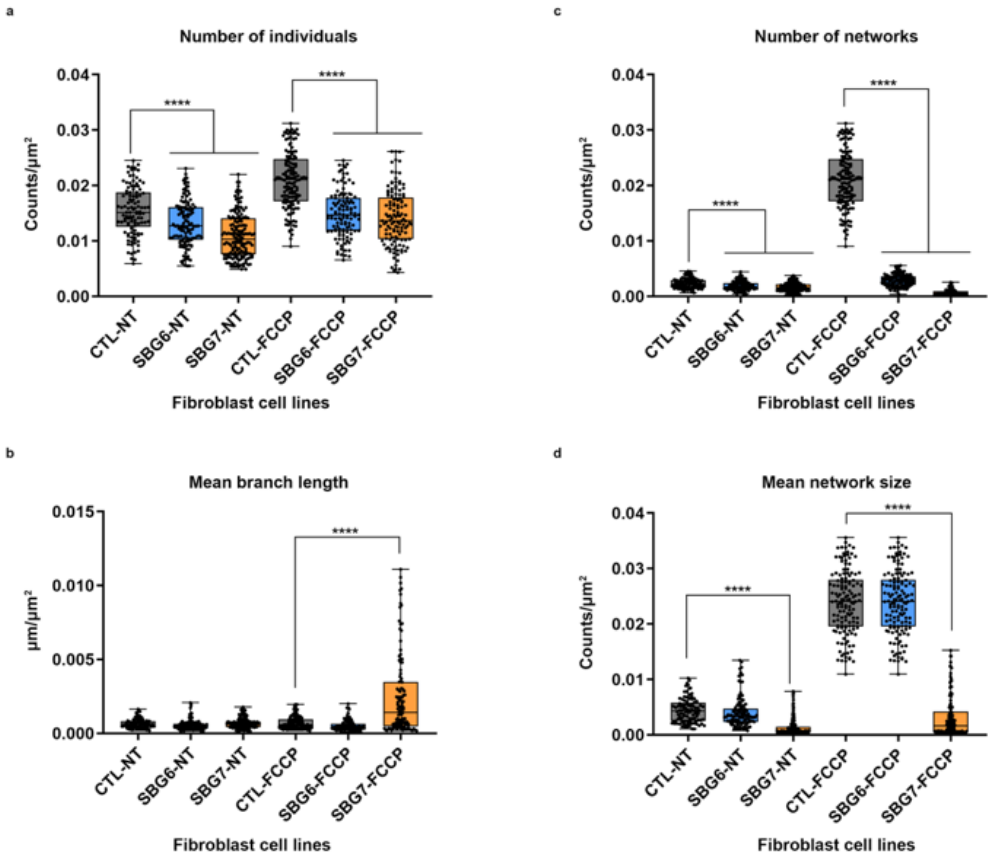

Figure 4. Mitochondrial Structure of Diseased and Healthy Fibroblast. Phase contrast, MitoTracker Red fluorescent, and Skeletonized images of the control and diseased cell lines. Graphs comparing the means of a)Number of Individuals, b) Mean branch length, c) Number of networks, and d) Mean network size between the control group and diseased cell lines in presence and absence of FCCP. Data represents 5 biological replicates for control and diseased cell lines. p* <0.05, **<0.01, ***<0.001, and ****<0.0001

Mitochondrial Membrane Potential is lower in tRNA mutant fibroblast cell lines:

To further test the hypothesis that a defect in mitochondrial morphology could correlate with a defect in the function of the mitochondria we recorded MMP in both tRNA mutant and healthy control fibroblast cell lines. Flow cytometry techniques was used to evaluate MMP, this result was further confirmed using immunocytochemistry and fluorescence

microscopy (Fig. 5). FCCP and Oligomycin treatments served as negative and positive controls in this experiment. Results from this experiment suggests a trend towards decreased MMP (Fig. 6) for both diseased cell lines relative to control.

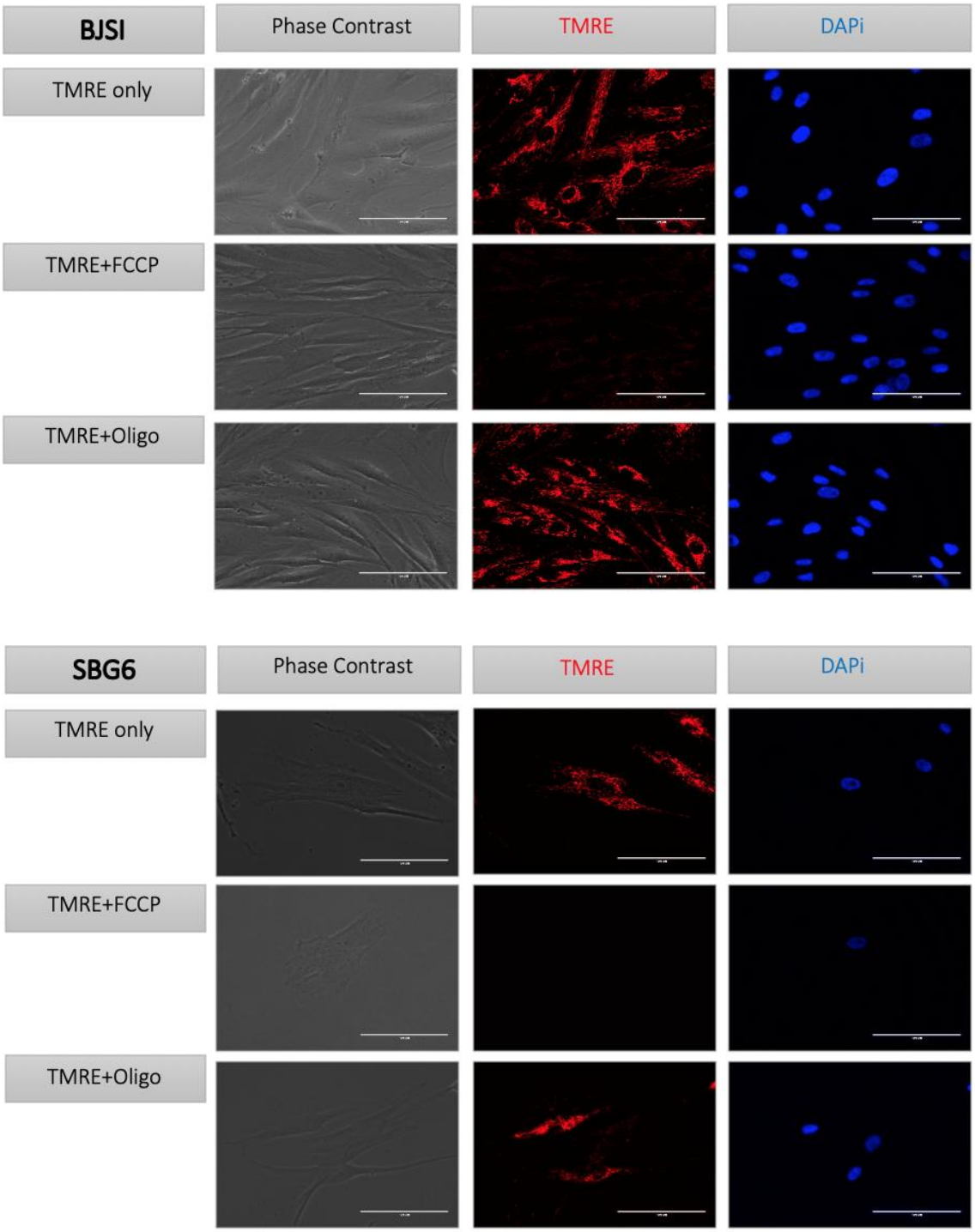

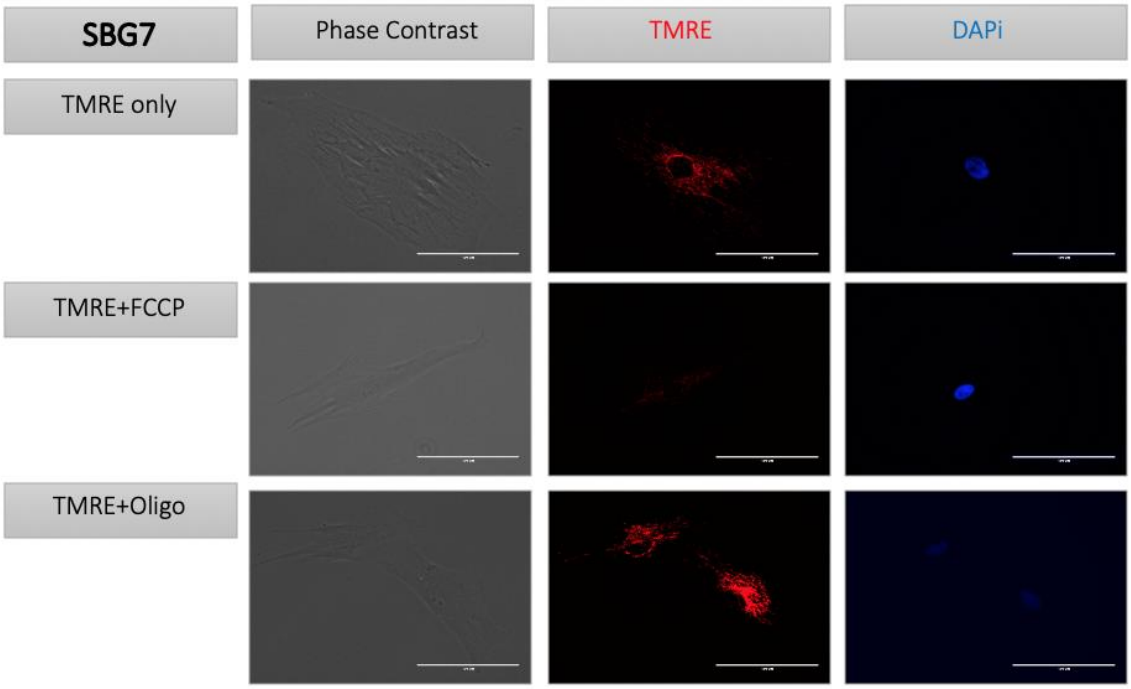

Figure 5. Lower fluorescent intensity observed in diseased cell lines compared to control cell line in the presence of mitochondrial complex inhibitors. Fibroblast cells images from diseased and control cell lines taken under phase contrast, Red Fluorescent Protein (RFP), and DAPi channels in the presence of TMRE only, TMRE + FCCP, and TMRE + Oligomycin.

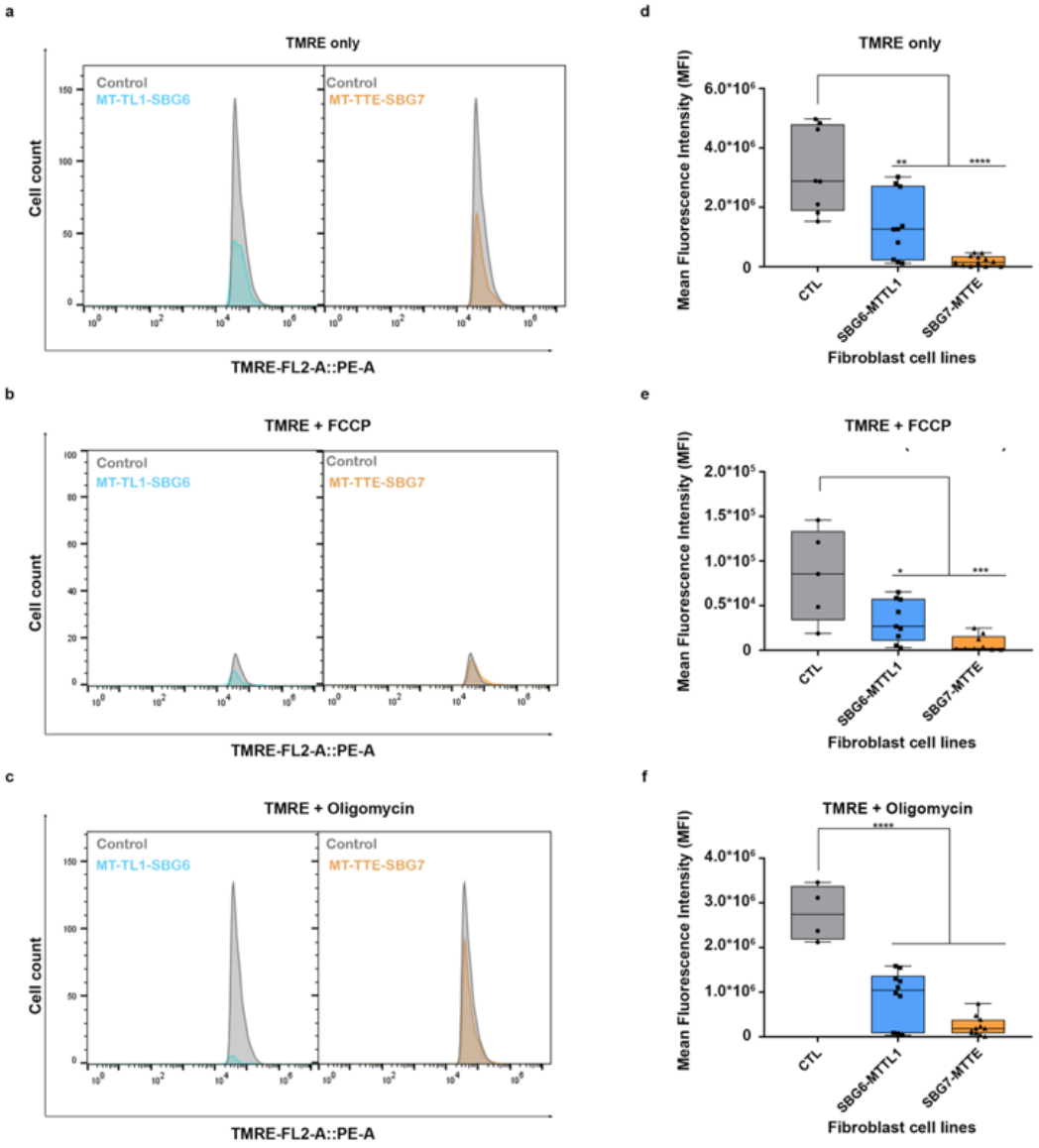

Figure 6. Diseased cell lines exhibit lower membrane potential than control cell line in the presence and absence of mitochondria toxins. Histogram showing the live TMRE positive cell population. Graphs comparing the means of the normalized mean fluorescent intensity values for the control cell line and the diseased cell lines in the presence of d) TMRE only, e) TMRE + FCCP, and f) TMRE + Oligomycin. Data represents 3 biological replicates for control and diseased cell lines. p* <0.05, **<0.01, ***<0.001, and ****<0.0001

Mitochondrial ROS is not altered in tRNA mutant cell lines

Finally, to understand the relationship between mitochondrial morphology and function,

we observed mitochondrial ROS production in diseased and healthy control fibroblast

cell lines. Flow cytometry techniques were used to evaluate MitoROS and results were further confirmed using immunocytochemistry and fluorescence microscopy (Fig. 7). Our results suggests a trend towards lower ROS production (Fig.8) in both diseased cell lines relative to control cell lines, however, these differences are not statistically significant. When we treated cells with mitochondrial inhibitors, Rotenone or AntimycinA, we found that the mean fluorescence intensity was significantly lower in both SBG6 and SBG7 compared to the control cell line (Fig. 8 e-f).

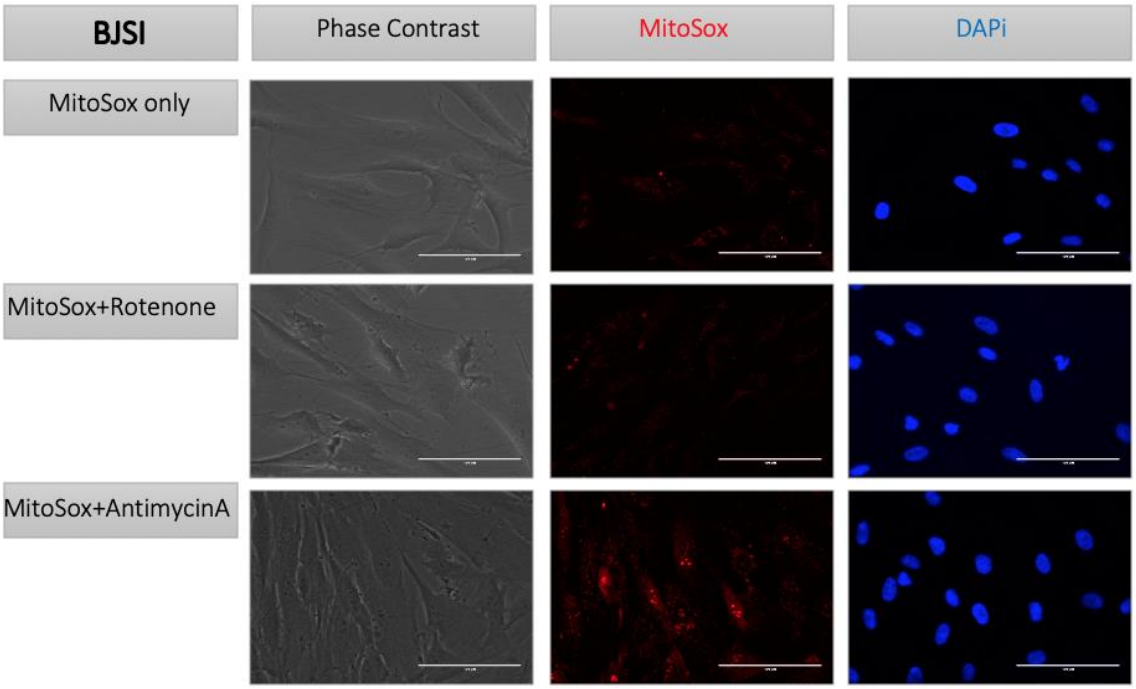

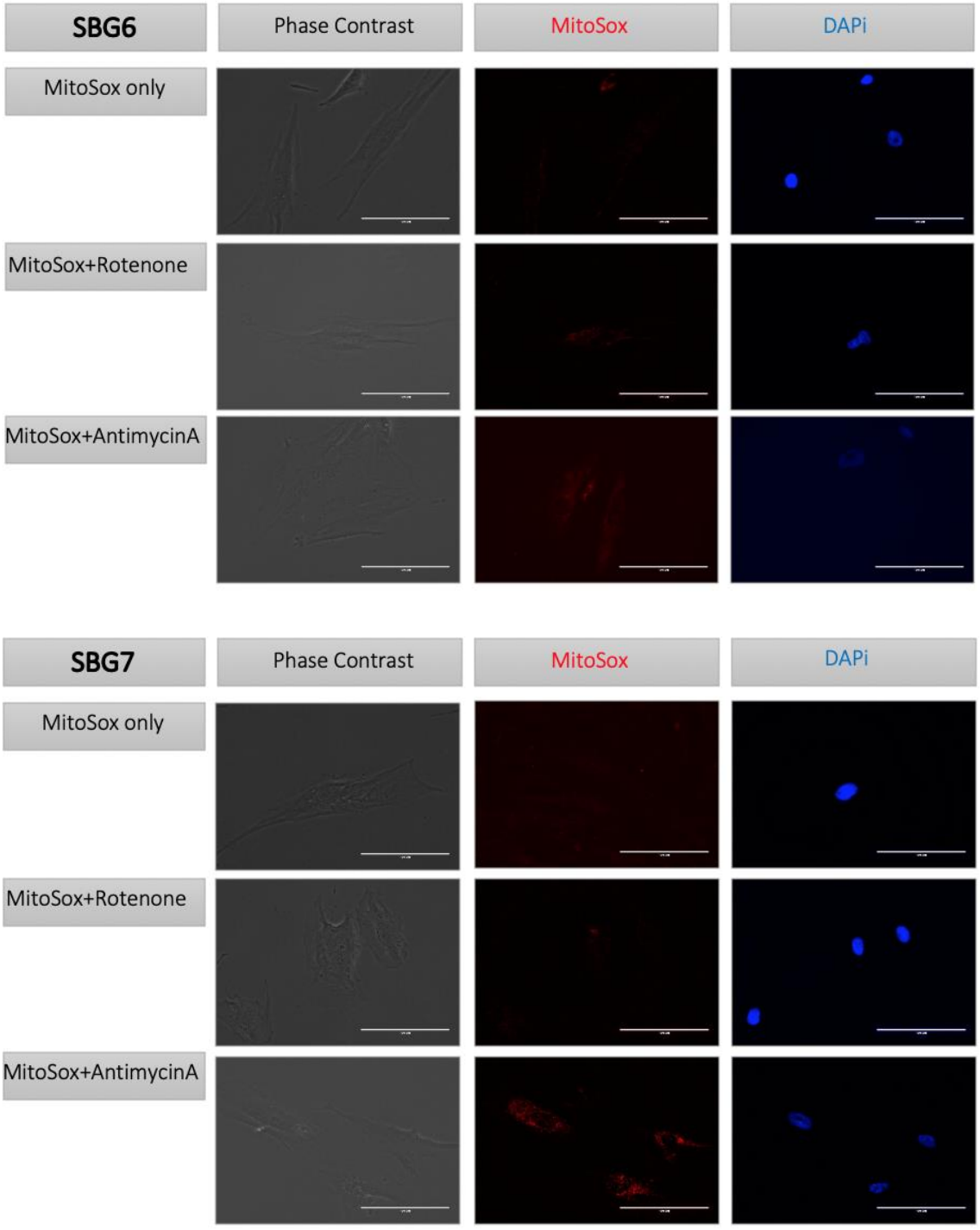

Figure 7. Fluorescent images of fibroblast cells in the presence of mitochondrial complex inhibitors. Fibroblast cells images from diseased and control cell lines taken under phase contrast, Red Fluorescent Protein (RFP), and DAPi channels in the presence of MitoSox only, MitoSox + Rotenone, and MitoSox + AntimycinA.

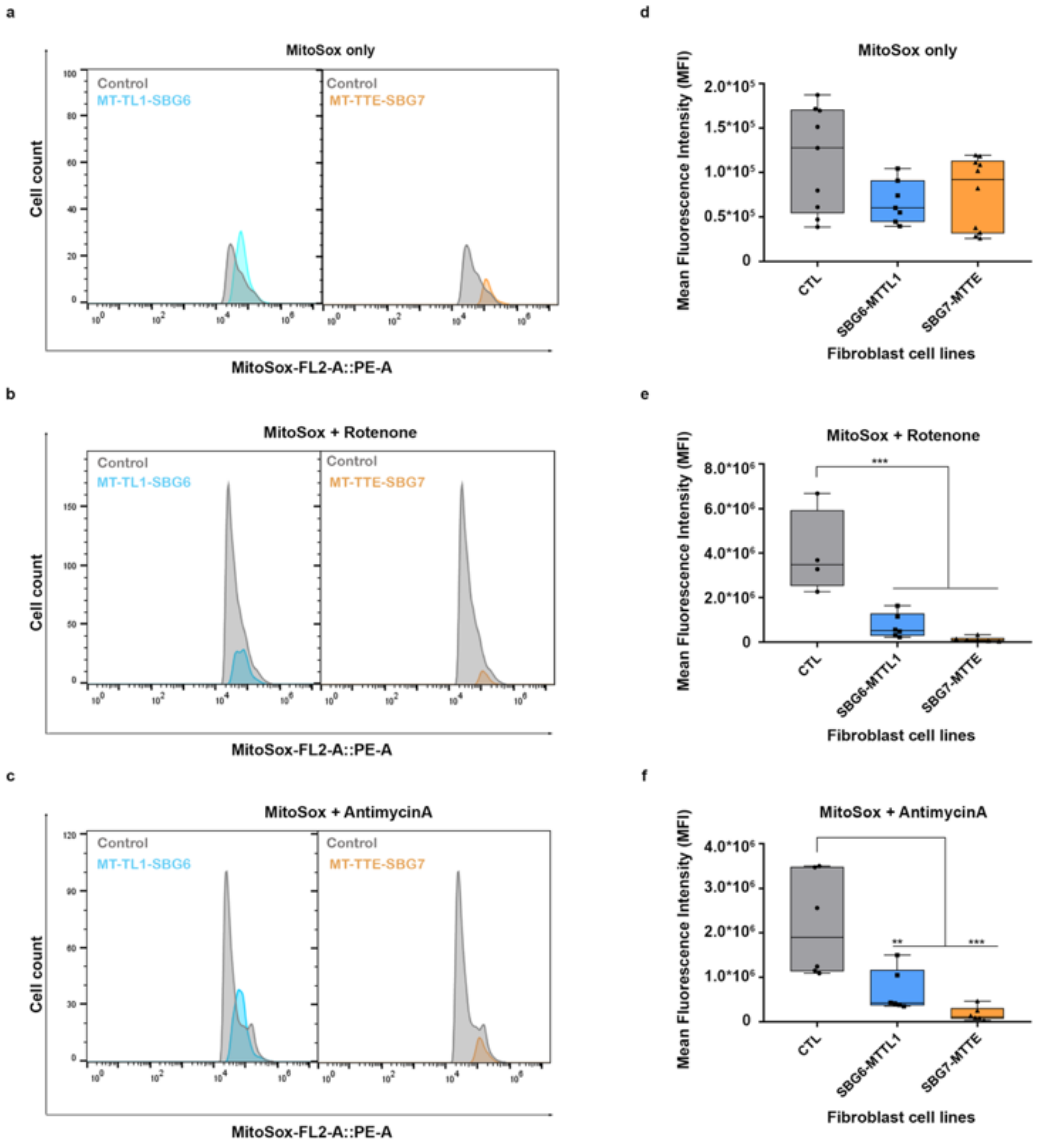

Figure 8. Diseased cell lines exhibit lower ROS production than control cell line only in the presence of mitochondrial complex inhibitors. Histogram showing the live MitoSox positive cell population. Graphs comparing the means of the normalized mean fluorescent intensity values for the control cell line and the diseased cell lines in the presence of d) MitoSox only, e) MitoSox + Rotenone, and f) MitoSox + Antimycin. Data represents 3 biological replicates for control and diseased cell lines. p* <0.05, **<0.01, ***<0.001, and ****<0.0001

Discussion

It has been suggested that mutations in mitochondrial DNA can lead to an imbalance in the cycle of fission and fusion, thereby altering the morphology of the mitochondrial network (Ni et al., 2015). We anticipated that the mutant tRNA cell lines would exhibit a a more fragmented (particularly in the presence of FCCP) or more fused mitochondrial network structure (Liesa & Shirihai, 2013). A hyper-fragmented network would be expected to result in increased count of mitochondria individuals as well as increased number of networks with subsequent decrease in mean branch length and network size, this would be the expected result with FCCP treatment (Valente et al., 2017). A hyper-fused network would be expected to exhibit a decreased count of mitochondria individuals and decreased number of networks with subsequent increase in mean branch lenth and network size. The number of individuals and the number of networks was lower in tRNA mutant cell lines than the control with and without FCCP treatment, suggesting a more fused network. The mean branch length was significantly higher in SBG7, but the mean branch length of SBG6 was not significantly different from the control. The mean network size was significantly lower in SBG7, yet SBG6 was again not significantly different than the control. The results suggest that the tRNA mutant cell lines exhibit a different morphology than the control cell line. While SBG7 shows a trend towards fusion, SBG6 was more like the control. The similarity between SBG6 and healthy control could suggest that the mutation load is lower in this cell line.

Healthy mitochondria maintain a membrane potential across the inner mitochondrial membrane in order to provide energy to drive ATP synthesis (Chen, 1988). In addition to the structural analysis, we sought to understand if structural differences in

these mutant cell lines would translate to functional defect. To do this we examined mitochondrial membrane potential (MMP). Moreover, FCCP and Oligomycin were used to serve as negative and positive controls respectively. FCCP destabilizes the proton gradient across the inner membrane space (Brennan et al., 2006) as a result dissipating the membrane potential. Oligomycin inhibits ATP synthase by blocking the proton pump, thereby hyperpolarizing the membrane. (Fernyhough & McGavock, 2014). We hypothesized that tRNA mutant cell lines would display decreased mitochondrial function, which may be indicated by a lower mitochondrial membrane potential. Flow cytometry analysis showed that tRNA mutant cell lines exhibited lower MMP relative to the healthy control cell line. Since the mitochondrial tRNA is involved in translation of proteins, enzymatic functions of many of the complexes involved in OxPhos could potentially be perturbed, owing to incorporation of dysfunctional proteins (Pek et al., 2019). Therefore, we anticipate that the defects caused by tRNA mutations may cause overall decrease in OxPhos activity. This could explain our findings of reduced membrane potential in tRNA mutant cell lines. These results do not show the typical mitochondrial response to Oligomycin, as control cell line does not display notably higher mitochondrial membrane potential. Further experiments will need to be conducted in order to confirm the hyperpolarizing action of Oligomycin.

Finally, we assessed mitochondrial ROS production as a second measure of mitochondrial function. ROS are created during normal respiration by the reduction of oxygen (Murphy, 2009). ROS production has been reported to serve as a means of communication between mitochondria and the nucleus in healthy cells (Murphy, 2009). Unusually high or unusually low level of ROS can thus serve as an indicator of a diseased

state. We would expect that mitochondrial disease would result in ROS levels that differ from those of control. Flow cytometry analysis indicated that a trend exists towards lower ROS production in tRNA mutant cell lines, however the results were not statisically significant.

In order to confirm the flow cytometry data and its assertions about mitochondrial function, we used immunocyochemistry and fluorescent microscopy to measure mitochondrial membrane potential and ROS production. The results showed that the tRNA mutant cell lines displayed decreased membrane potential compared to control in all treatment groups (Supp. Fig. 1). The tRNA mutant cell lines exhibited a trend of decreased ROS production (Supp. Fig. 2) compared to the control, but it was not significant. This data supports our flow cytometry results.

Morphological analysis of mitochondrial structure in this study showed an altered morphology in tRNA mutant cell lines compared to the control. The functional analysis of diseased mitochondria indicated that tRNA mutant cell lines exhibit decreased function in terms of mitochondrial membrane potential, but not in regards to ROS production. Further investigation into how tRNA mutations affect the respiratory chain could help to shed light on which aspects of the mitochondria may be directly affected. It is worthwhile to mention that the MiNA software does not distinguish between rods and punctate shapes, perhaps writing a code for this distinction could be beneficial in determining the differences between diseased and healthy cell lines.

Supplementary Figures

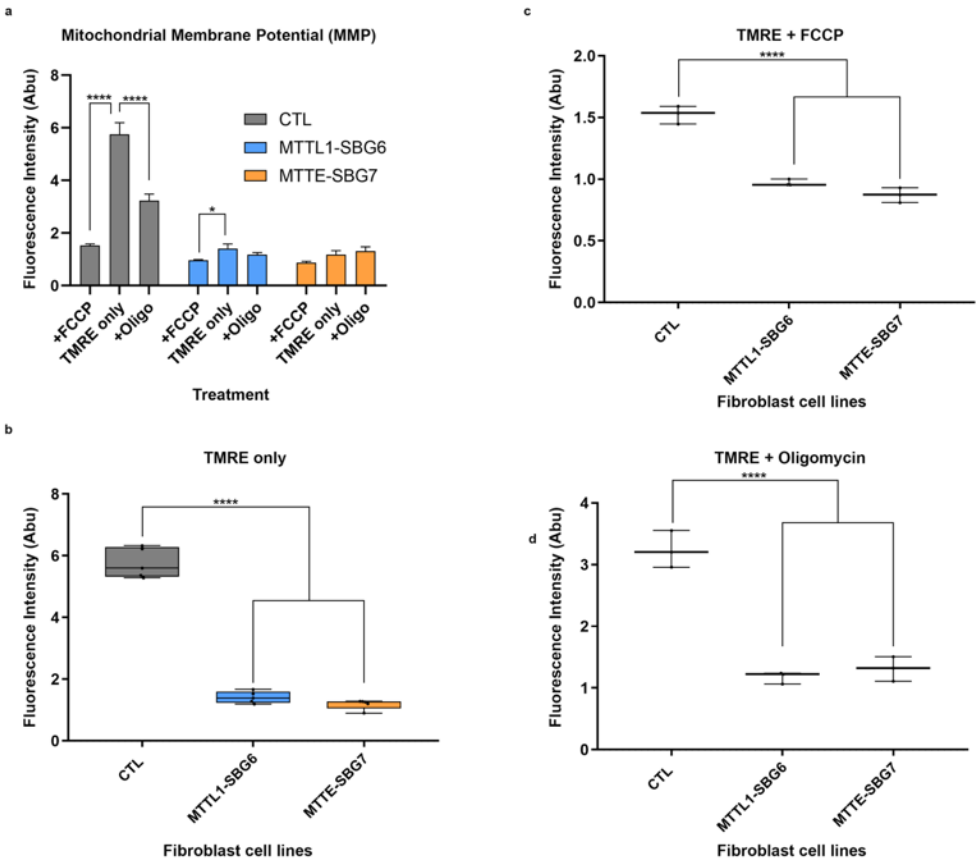

Supplementary Figure 1. Diseased cell lines exhibit lower membrane potential than control cell line in the presence and absence of mitochondrial toxins. Graphs comparing the means of the fluorescent intensity between the control and diseased cell lines in the presence of b) TMRE only, c) TMRE + FCCP, and d) TMRE + Oligomycin. Data represents 3 biological replicates for control and diseased cell lines. p* <0.05, **<0.01, ***<0.001, and ****<0.0001

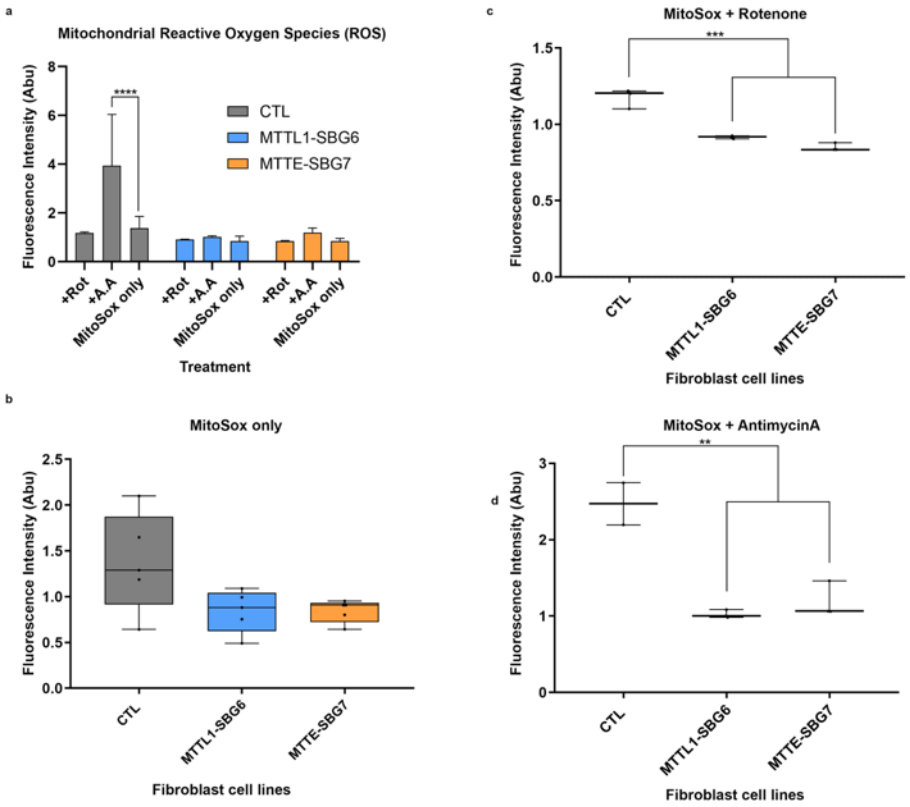

Supplementary Figure 2. Diseased cell lines exhibit lower ROS production than control cell line in the presence of mitochondrial complex inhibitors. Graphs comparing the means of the fluorescent intensity between the control and diseased cell lines in the presence of b) MitoSox only, c) MitoSox+Rotenone, and d) MitoSox+AntimycinA. Data represents 3 biological replicates for control and diseased cell lines. p* <0.05, **<0.01, ***<0.001, and ****<0.0001

References

Brennan, J. P., Southworth, R., Medina, R. A., Davidson, S. M., Duchen, M. R., & Shattock, M. J. (2006). Mitochondrial uncoupling, with low concentration FCCP, induces ROS-dependent cardioprotection independent of KATP channel activation. *Cardiovascular Research*. https://doi.org/10.1016/j.cardiores.2006.07.019

Cadenas, S. (2018). Mitochondrial uncoupling, ROS generation and cardioprotection. *Biochimica et Biophysica Acta - Bioenergetics*. https://doi.org/10.1016/j.bbabio.2018.05.019

Chen, L. B. (1988). Mitochondrial membrane potential in living cells. *Annual Review of Cell Biology*. https://doi.org/10.1146/annurev.cb.04.110188.001103

El-Hattab, A. W., Adesina, A. M., Jones, J., & Scaglia, F. (2015). MELAS syndrome: Clinical manifestations, pathogenesis, and treatment options. *Molecular Genetics and Metabolism*. https://doi.org/10.1016/j.ymgme.2015.06.004

Fernyhough, P., & McGavock, J. (2014). Mechanisms of disease: Mitochondrial dysfunction in sensory neuropathy and other complications in diabetes. In *Handbook of Clinical Neurology*. https://doi.org/10.1016/B978-0-444-53480-4.00027-8

Gupta, R. C., & Milatovic, D. (2014). Insecticides. In *Biomarkers in Toxicology*. https://doi.org/10.1016/B978-0-12-404630-6.00023-3

Koga, S. J., Hodges, M., Markin, C., & Gorman, P. (1995). MELAS syndrome. *The Western Journal of Medicine*. https://doi.org/10.15844/pedneurbriefs-1-4-6

Liesa, M., & Shirihai, O. S. (2013). Mitochondrial dynamics in the regulation of nutrient utilization and energy expenditure. *Cell Metabolism*. https://doi.org/10.1016/j.cmet.2013.03.002

Murphy, M. P. (2009). How mitochondria produce reactive oxygen species. *Biochemical Journal*. https://doi.org/10.1042/BJ20081386

Ni, H. M., Williams, J. A., & Ding, W. X. (2015). Mitochondrial dynamics and mitochondrial quality control. *Redox Biology*. https://doi.org/10.1016/j.redox.2014.11.006

Nicholls, D. G., & Ferguson, S. (2013). *Bioenergetics: Fourth Edition*. *Bioenergetics: Fourth Edition*. https://doi.org/10.1016/C2010-0-64902-9

Pek, N. M. Q., Phua, Q. H., Ho, B. X., Pang, J. K. S., Hor, J. H., An, O., … Soh, B. S. (2019). Mitochondrial 3243A > G mutation confers pro-atherogenic and pro-inflammatory properties in MELAS iPS derived endothelial cells. *Cell Death and Disease*. https://doi.org/10.1038/s41419-019-2036-9

Queen, R. A., Steyn, J. S., Lord, P., & Elson, J. L. (2017). Mitochondrial DNA sequence context in the penetrance of mitochondrial t-RNA mutations: A study across multiple lineages with diagnostic implications. *PLoS ONE*. https://doi.org/10.1371/journal.pone.0187862

Quinlan, C. L., Treberg, J. R., & Brand, M. D. (2011). Mechanisms of mitochondrial free radical production and their relationship to the aging process. In *Handbook of the Biology of Aging*. https://doi.org/10.1016/B978-0-12-378638-8.00003-8

Scaglia, F., & Wong, L. J. C. (2008). Human mitochondrial transfer RNAs: Role of pathogenic mutation in disease. *Muscle and Nerve*. https://doi.org/10.1002/mus.20917

Valente, A. J., Maddalena, L. A., Robb, E. L., Moradi, F., & Stuart, J. A. (2017). A simple ImageJ macro tool for analyzing mitochondrial network morphology in

mammalian cell culture. *Acta Histochemica*.

https://doi.org/10.1016/j.acthis.2017.03.001